JOURNAL OF GEOPHYSICAL RESEARCH, VOL. 113, C07030, doi:10.1029/2007JC004306, 2008

A coastal current in winter: Autonomous underwater vehicle observations of the coastal current east of Cape Cod

Andrey Y. Shcherbina[1,2] and Glen G. Gawarkiewicz[1]

Received 26 April 2007; revised 14 February 2008; accepted 18 April 2008; published 22 July 2008.

[1] Evolution of the coastal current structure on the shallow continental shelf east of Cape Cod was studied using autonomous underwater vehicle (AUV) surveys and moored observations during the winters of 2005 and 2006. A coastally bounded plume of relatively fresh water, characteristic of a coastal current, persisted throughout both winters despite strong mixing. Nondimensional parameter analysis classified the plume as a bottom-trapped gravity current over a moderately steep slope, placing it in the context of other buoyant coastal currents. The range of water properties within the coastal current, its spatial extent and temporal variability were characterized on the basis of the data from repeat hydrographic sections. Along-shore freshwater transport was dominated by highly variable barotropic flow driven by local wind and basin-wide pressure gradients. It eventually contributed substantially to the average southward along-shore freshwater transport, estimated at $1.1 \pm 0.3 \times 10^3$ m^3 s^{-1} in February and $1.8 \pm 0.4 \times 10^3$ m^3 s^{-1} in the first half of March 2006. The contribution of baroclinic buoyancy-driven freshwater transport was typically an order of magnitude lower during both winters. Despite the relative weakness of the baroclinic freshwater transport, the coastal current potentially had a major impact on water mass modification during the winter. Continual presence of the low-salinity plume prevented the formation of cold dense water near the coast and its export offshore. The coastal current effectively isolated the inner-shelf zone, reducing its potential role in ventilation of the intermediate layers of the Wilkinson Basin of the Gulf of Maine.

Citation: Shcherbina, A. Y., and G. G. Gawarkiewicz (2008), A coastal current in winter: Autonomous underwater vehicle observations of the coastal current east of Cape Cod, *J. Geophys. Res.*, *113*, C07030, doi:10.1029/2007JC004306.

1. Introduction

[2] The continental shelf is the central stage of water mass formation in the world's oceans. In shallow water, modification of thermohaline properties through the interaction with the atmosphere and the land is greatly amplified. Moreover, opposing influences often take place simultaneously or sequentially. For example, buoyancy input through the freshwater runoff may be followed by buoyancy loss due to intense cooling. These influences, however, are traditionally considered separately, which may obscure their interaction. In this study we investigate the effects of wintertime cooling in the presence of a buoyant coastal current.

[3] Fluxes of negative buoyancy due to surface cooling or brine rejection have the greatest impact on the shelf water mass formation. These processes create density anomalies that facilitate lateral advection and offshore transport of modified water masses. Numerical models and direct observations have identified eddy fluxes as a key mechanism to transport the density anomaly offshore [*Gawarkiewicz and Chapman*, 1995; *Pringle*, 2001; *Shcherbina et al.*, 2004].

[4] In many areas, modified shelf water penetrates stratification over the continental slope and adjoining basins, creating extensive layers of intermediate waters. Examples include the phenomena of the Arctic Ocean halocline, the North Pacific Intermediate Water, and the Cold Intermediate Layer in the Black Sea.

[5] In the Gulf of Maine in the northeast of the United States, the Maine Intermediate Water (MIW) is believed to be formed in winter in the shallow regions on the western edge of the Gulf [*Brown et al.*, 1977; *Brown and Irish*, 1993; *Hopkins and Garfield*, 1979]. *Mupparapu and Brown* [2002] have shown that one-dimensional mixed layer models do not produce sufficiently large heat exchange between 60 and 160 m depth to explain their observations. There is thus a negative heat content anomaly that they suggest is formed in shallow waters to the west. While this problem has been identified for some time, there has been little work to identify either the actual geographical regions which contain cold water masses or the specific processes which contribute to the formation of cold water masses.

[6] In search of the potential source of modified cold dense shelf water in the western Gulf of Maine, we

[1]Woods Hole Oceanographic Institution, Woods Hole, Massachusetts, USA.

[2]Now at Applied Physics Laboratory, University of Washington, Seattle, Washington, USA.

0148-0227/08/2007JC004306$09.00

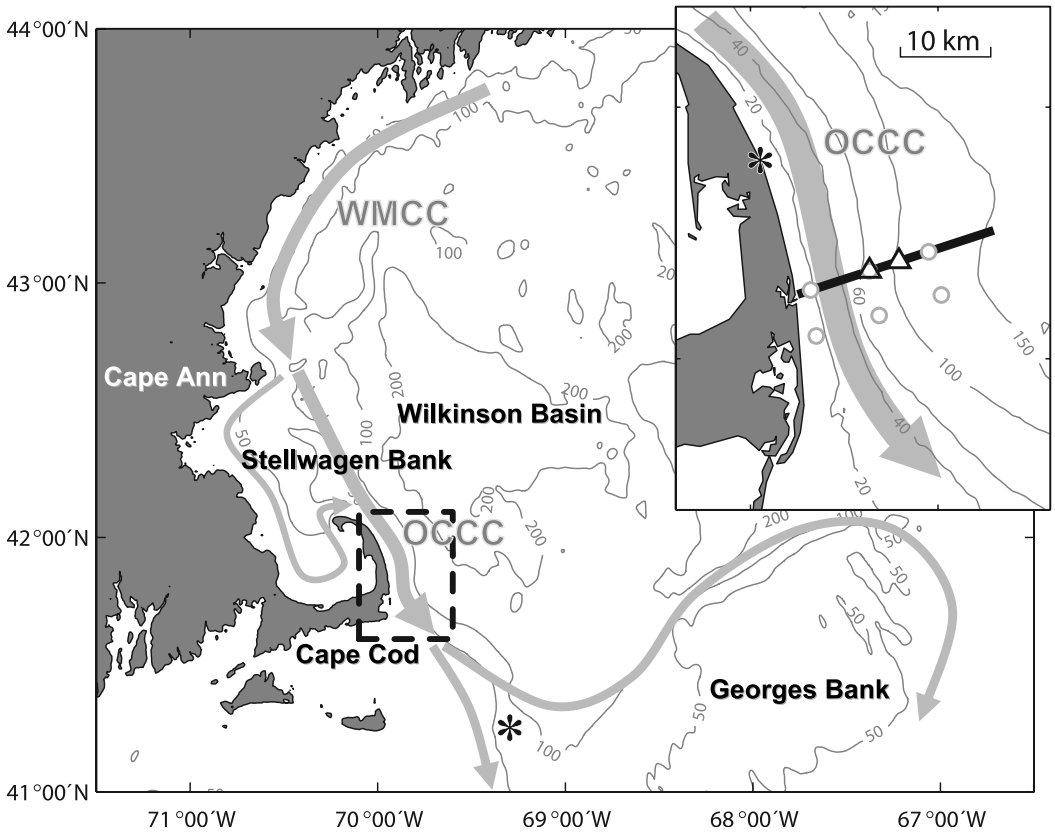

Figure 1. Map of the southwestern Gulf of Maine. Dashed box marks the Outer Cape Cod region, also shown on the inset. The inset shows the REMUS survey track (black line) for the 2006 field season, and the location of the bottom-mounted current profilers (triangles). The surface mooring array (gray circles) is also shown for the reference. Asterisks mark the locations of wind observations. Gray arrows show the schematics of the coastal current system, including Western Maine Coastal Current (WMCC) and Outer Cape Coastal Current (OCCC).

investigated the shelf area east of Cape Cod. The local area is shallow, reasonably distant from any major rivers entering the Gulf of Maine, and showing signs of low-temperature bands adjacent to the shore in satellite thermal imagery. However, we discovered that even in winter the shelf east of Cape Cod contained a well-developed coastal current, an extension of the Western Maine Coastal Current (WMCC) [*Geyer et al.*, 2004]. As shown below, this coastal current has an important impact on the processes of nearshore water mass modification.

[7] For the purpose of this discussion, we will refer to the nearshore flow east of Cape Cod as the Outer Cape Coastal Current (OCCC) although we recognize that this is a segment in a Gulf of Maine wide system of coastal currents [*Fong et al.*, 1997; *Franks and Anderson*, 1992; *Geyer et al.*, 2004]. This buoyant flow is driven by a freshwater anomaly originating on the Scotian shelf and supplemented by local river runoff [*Brown and Irish*, 1992; *Geyer et al.*, 2004; *Pettigrew et al.*, 1998]. North of Cape Cod the coastal current may follow two paths, bifurcating at Cape Ann: one following the Massachusetts Bay coastline, and the other cutting across along the eastern flank of Stellwagen Bank (Figure 1). The inshore branch is the weaker of the two and exhibits strong seasonal variability [*Signell et al.*, 1996]. The two branches rejoin to form the OCCC east of Cape Cod. South of Cape Cod, the OCCC splits again into two branches, one following the coastline south and west, and the other circling Georges Bank [*Chen et al.*, 1995a, 1995b; *Lynch et al.*, 1997; *Pettigrew et al.*, 2005].

[8] The OCCC is one of the major conduits of freshwater and nutrient exchange between the Gulf of Maine and the Middle Atlantic Bight. Wintertime freshwater transport of the OCCC has never been previously studied, probably since the current was assumed to disappear in winter. There are several direct estimates of the water and tracer transports by the coastal current in spring and summer, with which our results can be compared. OCCC hydrography and current structure was investigated during the South Channel Ocean Productivity Experiment (SCOPEX) [*Chen et al.*, 1995a, 1995b]. Even though the fresh water transport was not calculated, it can be inferred from the total volume and salt transports of the low-salinity plume, cited by *Chen et al.* [1995b]. On the basis of SCOPEX data, fresh water transports were $(1.0 \pm 0.4) \times 10^3$ m^3 s^{-1} for the April 1988 survey, and $(6 \pm 3) \times 10^3$ m^3 s^{-1} in June 1989. *Geyer et al.* [2004] studied the freshwater transport of the Gulf of Maine Coastal Current at Cape Porpoise (43°20′N), upstream of OCCC. They observed the transport increasing from around 2×10^3 m^3 s^{-1} in March and April of 1994 to over 9×10^3 m^3 s^{-1} in early May, before dropping sharply to

Table 1. Characteristic Bottom Slope and Slope Burger Number $Sl = \alpha N/f$ for Several Coastal Current Regions Previously Studied[a]

Study Area	Bottom Slope (α)	Slope Burger Number
North California shelf, CODE-1 site (LT91)	3.5×10^{-2}	2.5
San Diego shelf (LW86)	1.8×10^{-2}	no data
Oregon shelf (Ka05)	1.2×10^{-2}	no data
Outer Cape Cod shelf (present study)	$\mathbf{7.0 \times 10^{-3}}$	**0.4**
North Carolina shelf (LL06, Ra99)	3.6×10^{-3}	0.7
Gulf of Maine shelf (BB78)	3.0×10^{-3}	0.3
New Jersey shelf, LEO-15 site (G04, Ta99)	1.0×10^{-3}	0.8

[a] N is the typical buoyancy frequency; f is the Coriolis parameter. The present experiment is in bold, and citations are abbreviated as follows: L91, *Lentz and Trowbridge* [1991]; LW86, *Lentz and Winant* [1986]; Ka05, *Kirincich et al.* [2005]; LL06, *Lentz and Largier* [2006]; Ra99, *Rennie et al.* [1999]; G04, *Garvine* [2004]; Ta99, *Traykovski et al.* [1999]; and BB78, *Brown and Beardsley* [1978].

less than 0.5×10^3 m^3 s^{-1} in June. Mean transport during the freshet period of 1994 (end of March–June) was 2.8×10^3 m^3 s^{-1}.

[9] The buoyant coastal current presents a barrier for the cross-shelf water mass exchange. The plume of relatively fresh water associated with the current contains positively buoyant water adjacent to the coast. Before the export of dense water from the shallows can start, the negative buoyancy forcing associated with cooling must reverse the cross-shelf density gradients. It is presently not known whether this takes place on the Outer Cape shelf or elsewhere, as systematic wintertime observations are scarce.

[10] In this paper, we will investigate the structure of the coastal current and its evolution throughout the winter. Section 2 is a description of the components of the field program including the autonomous underwater vehicle (AUV) used for high-resolution hydrographic surveys. The coastal current thermohaline structure and its evolution is presented in section 3. The freshwater transport, including both baroclinic and barotropic contributions to the along-shelf flow, appear in section 4. The discussion in section 5 focuses on the influence of a coastal current on formation and export of dense shelf waters. Conclusions are briefly stated in section 6.

2. Outer Cape Field Observations

[11] The present study focuses on the shelf east of Cape Cod, MA (Figure 1). The experimental domain extended approximately 15 km offshore and spanned the depth range of 10–120 m. The offshore edge of the domain was limited by the presence of a major shipping lane running south from Boston. The typical bottom slope in this region was 7×10^{-3}. This value is intermediate between steep western U.S. shelves and more gentle U.S. east coast shelves that have been extensively studied (Table 1).

[12] The Outer Cape Cod coastline is oriented roughly in the north-south direction. For the purpose of this study we will use an along-shore coordinate system, based on polarization of vertically averaged and low-passed (subtidal) flow [*Kundu and Allen*, 1976; *Lentz*, 2001]. The major axis of the variance ellipse of the observed flow (section 2.2) pointed to 348° true and defined the along-shore axis. The orthogonal across-shore axis then pointed to 78° true.

[13] In situ observations of the wintertime evolution of OCCC were made during the two wintertime field seasons. The 2006 field season mooring array, deployed from 19 December 2005 to 21 March 2006, consisted of 6 surface and 2 bottom moorings, arranged along two cross-shore lines (Figure 1). Moored observations were combined with routine hydrographic surveying along the northern line of moorings. The orientation of the survey line (72° true), determined by the local bathymetry, was close to the cross-shore axis direction (78° true) defined above. An abbreviated version of the experiment had been run during the previous year. The 2005 pilot study consisted of three surface moorings, but only one mooring survived the winter.

[14] The study heavily relied on AUV observations of the hydrographic and velocity structures on the shelf. Compared to shipboard casts, AUV allowed high-resolution profiling while minimizing deck operations. This allowed us to use smaller coastal vessels and work in higher sea states, both factors crucial for this study. When conditions allowed, concurrent shipboard operations complemented the AUV surveying.

[15] The present paper investigates the evolution of thermohaline structure of the coastal current and its freshwater transport based on the data of AUV hydrographic surveys, a moored velocity record, and meteorological observations. The following sections provide a detailed description of these data. Moored temperature observations are considered in a separate study (A. Y. Shcherbina and G. G. Gawarkiewicz, A coastal current in winter: 2. Wind forcing and cooling of a coastal current east of Cape Cod, submitted to *Journal of Geophysical Research*, 2008).

2.1. Autonomous Underwater Vehicle Observations

[16] High resolution cross-shelf surveying of the coastal current properties were performed by a specially equipped Remote Environmental Monitoring Unit (REMUS 100). REMUS is a compact light-weight self-propelled autonomous underwater vehicle (AUV), designed for operation in shallow water environments [*Moline et al.*, 2005]. A typical REMUS mission for the present study was a straight cross-shore section extending from the coast to approximately 25 km offshore along the northern line of moorings. The vehicle was programmed to follow a saw-tooth path through the water column, undulating from near-surface to 2 m above the bottom or its maximum operating depth of 90 m. Horizontal separation between the consecutive upward and downward tracks varied from 200 m in shallow water to 2 km at maximum dive depth. AUV REMUS was deployed and recovered using the 60-foot coastal research vessel *Tioga*. During the REMUS missions, *Tioga* provided acoustic and satellite tracking of the AUV and performed additional hydrographic surveying.

[17] The configuration and equipment of the AUV REMUS used in the present study has been optimized to enhance its long-range hydrographic surveying capabilities. The vehicle carried a high-accuracy external pumped Seabird SBE49 "FastCAT" conductivity-temperature-depth

(CTD) probe. The CTD data were recorded internally at the rate of 5 Hz. Nominal accuracy of SBE49 is ±0.002°C, ±0.0003 S m^{-1}, and $\pm 10^3$ Pa for temperature, conductivity, and pressure, respectively.

[18] To extend the surveys below the 90-m depth limit of the REMUS, a series of casts with a vessel-based Seabird SBE9 CTD profiler were performed at the offshore end of some of the REMUS transects while the AUV surveyed the shallower part of the sections. The data were subsequently merged and interpolated on a regular cross-shore section grid. Both CTDs used for the study had been recently calibrated by Seabird, making cross calibration unnecessary. Good agreement between the ship-based hydrographic casts and AUV surveying was verified using a few colocated profiles (not shown).

[19] A dual-head RDI Workhorse Navigator 1200 kHz acoustic Doppler current profiler (ADCP) measured the water velocity relative to the vehicle in a swath, extending approximately 15 m above and below the path of travel. Velocity profiling from a moving platform requires precise information on the vehicle motion relative to the Earth.

[20] To facilitate the midwater navigation capabilities, the REMUS used in the present study has been equipped with the Kearfott T-16B inertial navigation system (INS). The INS substantially improved the vehicle navigation by reducing the typical heading error by an order of magnitude, compared to the regular fluxgate compass. At the time of the experiment, however, the INS provided the vehicle attitude information but not the translational velocities owing to a conflict with the ADCP water profiling mode. As a result, the vehicle was essentially dead-reckoning its position while undulating beneath the surface. The vehicle velocities used for DR were obtained from the ADCP bottom tracking or crudely estimated from the propeller turn count when the bottom was beyond ADCP range.

[21] Accumulation of system errors required periodic surfacing of the vehicle, during which the global positioning system (GPS) fixes were used to reset the position estimated by DR. The frequency and the extent of the corrections depended on availability of ADCP bottom tracking, ambient currents, and the mission plan. During postprocessing, the navigation discontinuities, resulting from the GPS position updates, were identified and distributed uniformly over the preceding DR intervals. Vehicle velocities with respect to the Earth were also adjusted accordingly. In reality, navigation error accumulation is nonlinear, depending on ambient water speed and the vehicle path. Consequently, ADCP velocity measurements referenced to the linearly corrected vehicle velocity were slightly discontinuous over GPS position updates. On the basis of the typical value of such discontinuities, we estimate the remainder ADCP velocity error to be on the order of 0.05 m s^{-1}.

2.2. Moored Observations

[22] During the 2006 field season, a pair of bottom-mounted upward looking Acoustic Doppler Current Profilers (ADCPs) were deployed at the survey line (Figure 1). Upward looking 300-kHz RDI Workhorse ADCPs were used, set to measure water velocity in 2-m depth bins. Data were averaged over 10-min ensembles, each consisting of 80 individual measurements (“pings”). With these settings, nominal standard deviation of measured velocity is 7×10^{-3} m s^{-1} (RD Instruments WorkHorse Installation Guide, p/n 957-6152-00 (August 2002)).

[23] The instruments were housed in trawl-resistant bottom mountings (TRBMs), placed on the bottom at approximately 60- and 100-m depth (at 20 and 24 km offshore, respectively) along the northern mooring line (Figure 1). Owing to the heavy seas during the deployment and TRBM kiting, neither ADCP settled in the intended upright position on the bottom. As a result, the deeper instrument failed completely, while the shallower one became operational only from 1 February 2006 when it was presumably hit by a trawl and flipped upright. Overall, the deployment provided one velocity time series from the 60-m mooring site (41°50.128′N, 69°51.241′W) from 1 February to 21 March 2006.

2.3. Meteorological Observations

[24] Several sources of meteorological data were considered for this study (Figure 1). The closest meteorological station was located 17 km northwest of the middle of the mooring array in Wellfleet, Massachusetts. It is a land-based (30 m above sea level) commercial weather station operated by WeatherFlow, Inc. Simultaneous open ocean observations were available at the National Data Buoy Center station 44018, located 80 km southeast of the experiment site.

[25] Wellfleet observations appear to have been heavily influenced by coastal effects. The wind speed observed at this station was typically less than half of that reported by the offshore buoy (Figure 2). Shore-based data also showed signs of preferential shadowing at particular wind directions; northward and northwestward (upwelling favorable) winds were especially affected.

[26] Offshore buoy data were chosen as more representative of the shelf forcing, and were used in this study. Surface stress was estimated using the TOGA-COARE bulk air-sea flux algorithm [*Fairall et al.*, 2003]. The algorithm makes use of oceanographic and atmospheric conditions observed by the buoy to parameterize stability of the atmospheric boundary layer and estimate the appropriate wind drag coefficient.

[27] Wind-forcing in 2005–2006 was strongly seasonal. Upwelling-favorable northward winds prevailed in summer (June–September). In winter (December–March) the general wind direction became downwelling-favorable (southward). Periodic storms characterized by southwestward winds further intensified downwelling conditions in winter.

2.4. Freshwater Discharge Observations

[28] The Scotian shelf is the chief source of fresh water in the Gulf of Maine [*Brown and Irish*, 1993; *Pettigrew et al.*, 1998; *Smith*, 1983]. This inflow of low-salinity (31–33) shelf water is highly seasonal, with the wintertime maximum of about 0.3 Sv (1 Sv = 10^6 m^3 s^{-1}) and the mean annual transport of 0.14 Sv [*Smith*, 1983]. The WMCC plume is also fueled by the discharge from the St. John, Penobscot, Kennebec, Androscoggin, Saco, and Merrimack rivers [*Brown and Irish*, 1992; *Geyer et al.*, 2004; *Pettigrew et al.*, 1998]. The riverine fresh water outflow is also highly variable, but much better documented than the Scotian shelf input (Figure 3).

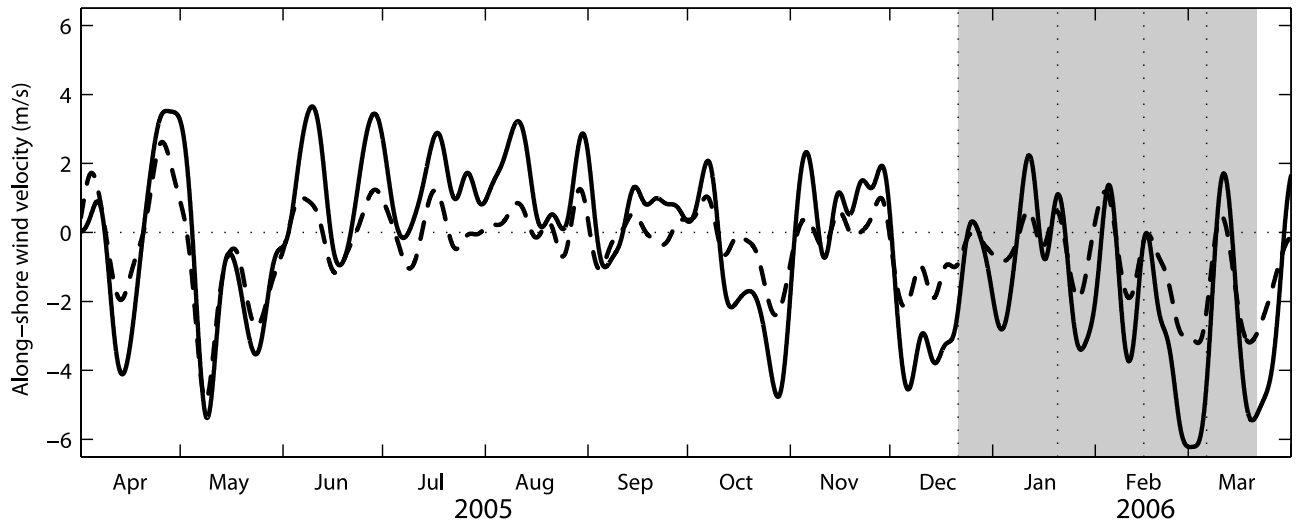

Figure 2. Alongshore wind in April 2005 to March 2006 based on an offshore buoy (solid line) and coastal (dashed line) observations. Hourly observations, low-passed with a 14-day Blackman filter are shown. Positive values correspond to the winds toward 348° true (approximately northward, upwelling favorable) winds. Gray shading represents the 2006 experiment duration. Vertical dashed lines mark REMUS surveys.

[29] The discharge time series (Figure 3) show stark contrast between our two field seasons. Cumulative freshwater input between November 2004 and March 2005 during the Winter 2005 study was 14 km^3, which was less than half of the 29 km^3 discharge during the corresponding period for the winter 2006 study. Discharge data for the St. John River (Canada), the largest single river flowing into the Gulf of Maine, were not available, but the water-level observations by Water Survey of Canada (http://www.wsc.ec.gc.ca), showed similar trends. The difference can be explained by the relatively milder winter of 2006, which had several freshet events in January and February, compared to 2005, when virtually no melting occurred until early April. It should be noted that during both the 2005 and 2006 winters, spanned by our observations, riverine freshwater input into the western Gulf of Maine was generally stronger than during the preceding years.

3. Coastal Current Structure in Winter

[30] The cross-shelf thermohaline structure observed on the Outer Cape Cod shelf in winter (Figures 4 and 5) was dominated by a wedge of relatively fresh water near the coast. Such structure is typical for a buoyant coastal current and is similar to that observed further upstream [*Geyer et al.*, 2004]. There are no major freshwater sources near the Outer Cape Cod, so the plume water observed there has undergone substantial modification since leaving the west-

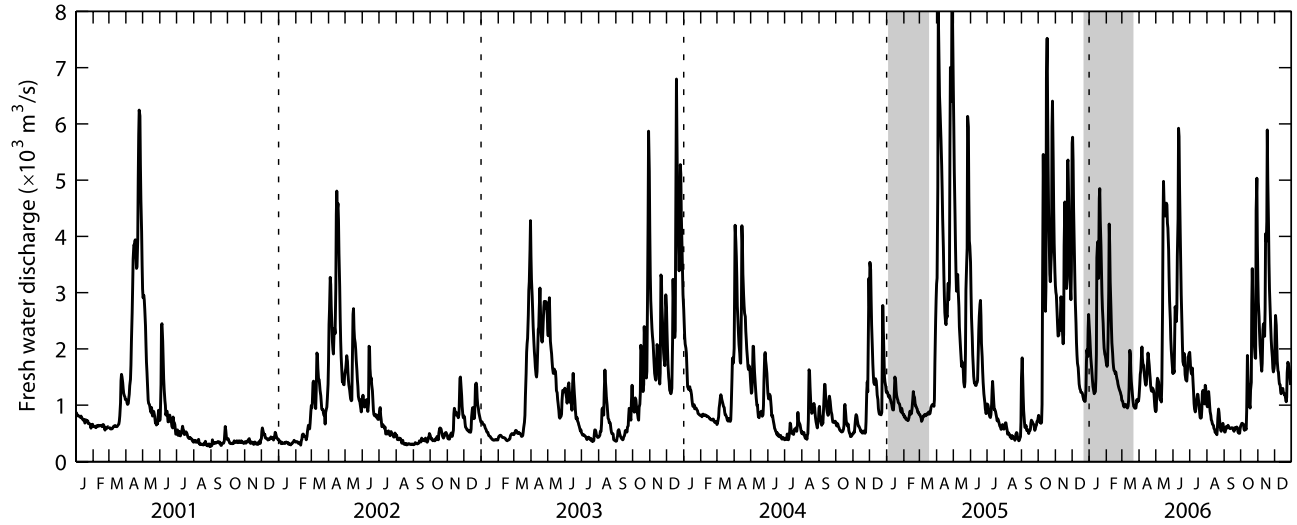

Figure 3. Combined fresh water discharge from Penobscot, Kennebec, Androscoggin, Saco, and Merrimack rivers, based on USGS daily data. Gray shading represents the duration of 2005 and 2006 experiments. Vertical dashed lines mark new years.

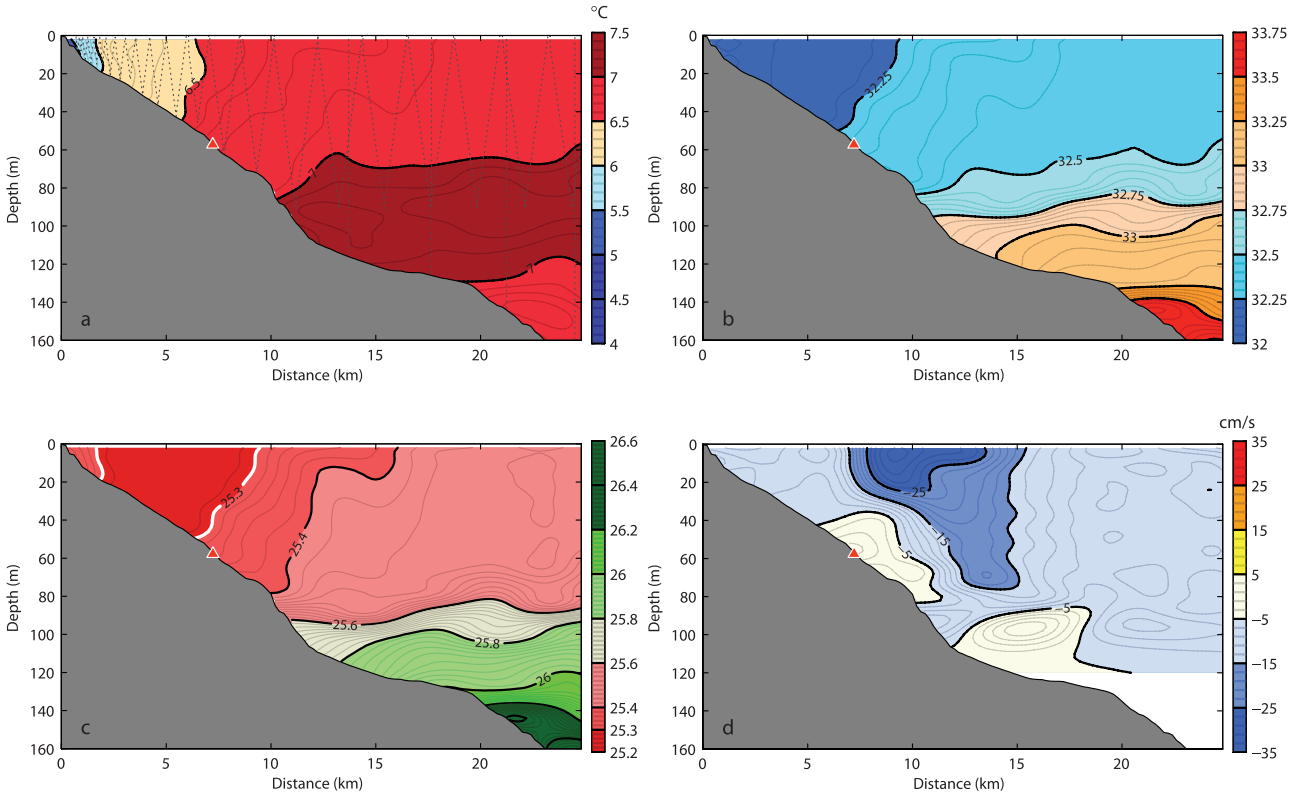

Figure 4. Distribution of (a) temperature, (b) salinity, (c) potential density, and (d) along-shore velocity on a cross-shelf section occupied on 21 December 2005 (basic state) with the REMUS AUV and shipboard CTD casts. AUV trajectory and locations of CTD casts are shown by dotted lines in Figure 4a. Position of the bottom mooring is indicated by red triangle. The thick white line in Figure 4c marks the estimated location of the OCCC front.

ern Gulf of Maine shelf. We shall refer to this modified plume as the "OCCC water," even though the maximum velocity axis of the coastal current is shifted toward the offshore edge of the plume.

[31] The offshore extent of the OCCC water was marked by a weak thermohaline front. A classical definition of a "front" implies order-of-magnitude enhancement of lateral gradients (R. W. Garvine, personal communication, 2007; M. Tomczak, unpublished lecture notes, http://gaea.es.flinders.edu.au/~mattom/ShelfCoast). In our observations, the surface density gradient within the OCCC was only 2–5 times stronger than the background. We shall still refer to this region of enhanced gradients as a "front," for consistency with similar studies.

[32] The shape of the freshwater wedge is expected to vary considerably with the changing alongshore wind [*Csanady*, 1978; *Lentz and Largier*, 2006]. This variability is discussed in the next section.

3.1. Cross-Shelf Thermohaline Structure: The Basic State

[33] We define the "basic state" thermohaline structure of the OCCC as that which was observed under low-wind conditions during the 21 December 2005 deployment cruise (Figure 4). In this state, frontal isopycnals intersected both the surface and the bottom, and were inclined with a slope of 0.017 (1°). The foot of the front was located at roughly the 60-m isobath, 7 km from the coast. In December of 2005 salinity inshore of the front was less than 32.2, compared to the offshore mixed layer salinity of about 32.45. The thermal front was less pronounced, with the temperature gradually increasing from 5.5°C near the coast to about 7°C offshore.

[34] Offshore of the OCCC front, a typical wintertime midshelf stratification was observed. It was characterized by a relatively thick surface mixed layer reaching to about 70 m. Stability of the water column was established by salinity increasing from 32.45 in the mixed layer to over 33.7 at 180 m depth. The temperature variations provided comparatively weaker contribution to the density stratification. Below the mixed layer, the temperature was increasing downward and reached a maximum of 7.3°C at about 90 m depth.

[35] Our OCCC basic state configuration corresponds to the "slope-controlled" (or "bottom-trapped") gravity current case, according to *Chapman and Lentz* [1994], *Yankovsky and Chapman* [1997], and *Lentz and Helfrich* [2002] classifications. The key nondimensional parameter distinguishing the surface- and bottom-trapped regimes of a plume away from the buoyant inflow is the ratio c_w/c_α, where $c_w = (g'h_p)^{1/2}$ and $c_\alpha = \alpha g'/f$ are the gravity current nose propagation speeds in limits of steep and gentle bottom slopes, respectively, $g' = g\Delta\rho/\rho_0$ is reduced gravity, h_p is the depth of the foot of the front, α is the bottom slope, f is the Coriolis parameter, g is the gravitational acceleration, $\Delta\rho = \rho_s - \rho_0$ is the density difference between the plume (ρ_s) and ambient (ρ_0) water [*Lentz and Helfrich*, 2002]. The

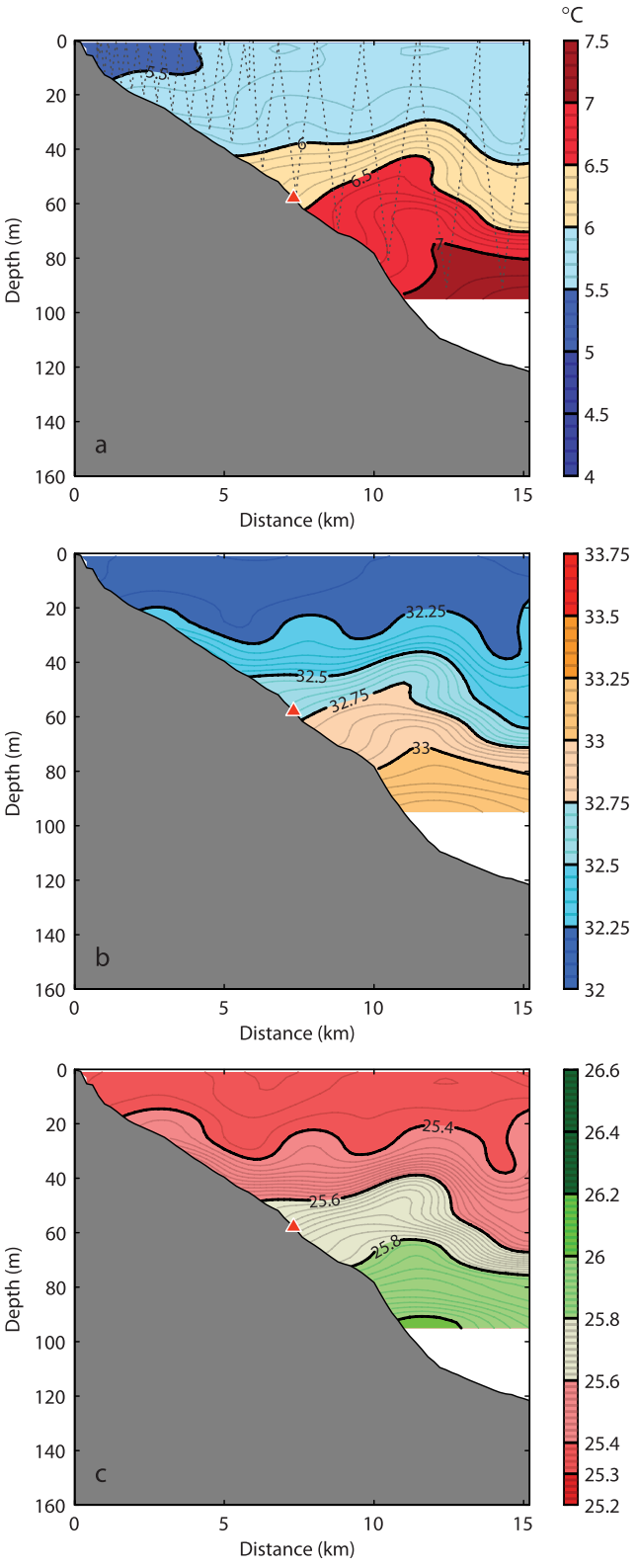

Figure 5. Distribution of (a) temperature, (b) salinity, and (c) potential density on a cross-shelf section occupied on 20 January 2006 (upwelling phase) with the REMUS AUV. The AUV trajectory is shown by dotted lines. Position of the bottom mooring is indicated by the red triangle.

ratio c_w/c_α can also be interpreted as an inverse of the slope Burger number $Sl = \alpha N/f$, where $N = (g'/h_p)$ is the buoyancy frequency. According to Lentz and Helfrich, a buoyancy current is slope-controlled if $c_w/c_\alpha \gg 1$, and surface-trapped if $c_w/c_\alpha \ll 1$. The OCCC structure in December 2005 corresponded to $c_w/c_\alpha = 2.6$, implying tendency toward the slope-controlled regime.

[36] As shown in the next section, thermohaline structure of the buoyant plume on the Outer Cape shelf was strongly influenced by the winds. This influence somewhat undermines the relevance of the *Lentz and Helfrich* [2002] scaling that considers the buoyancy effects alone.

3.2. Cross-Shelf Thermohaline Structure: Temporal Evolution

[37] The size and shape of a typical coastal current "wedge" on a cross-shelf section varies strongly. Changes of river runoff are expected to change the fresh water anomaly of the coastal current and its offshore extent. Wind-forcing primarily changes the slope of the front and along-shelf advection speed [*Blanton et al.*, 1989; *Csanady*, 1978; *Fong et al.*, 1997]. An apparent extreme of the OCCC configuration was observed on 20 January 2006 after a rare period of northward (upwelling favorable) winds (Figure 5). Contrary to the basic state (Figure 4), the coastal current front was almost horizontal and merged with the thermocline, as the freshwater plume was stretched offshore. Over the course of two field seasons, a range of intermediate OCCC configurations between these two extremes of downwelling and upwelling favorable winds were also observed.

[38] A simple objective procedure for determining the OCCC extent was necessary to facilitate tracking of the evolution of the coastal current. For the purpose of the present study, we treated the density front as the offshore boundary of the OCCC water. The front position, in turn, was determined by the isopycnal that corresponded to the maximum cross-shore gradient of surface density. This procedure enabled unique demarcation of the coastal current "wedge" on hydrographic sections (Figure 4c for an example) despite the changes of the coastal current salinity and temperature over the course of 2 years.

[39] The shape of the OCCC front varied substantially during the winters of 2005 and 2006 (Figure 6 and Table 2). Generally, the absolute value of the isopycnal slope was on the order of 1×10^{-2} during downwelling winds, and less than 3×10^{-3} during upwelling. Owing to the small number of available sections, we were unable to observe a clear correlation of the front slope with the wind stress magnitude similar to that demonstrated by *Lentz and Largier* [2006] for the Chesapeake Bay plume. General behavior of both coastal currents was analogous, except that the typical isopycnal slope of OCCC front is about 5 times greater than that of the Chesapeake plume.

[40] Section-averaged salinity of the OCCC water showed similar behavior in both winters (Figure 7). It stayed relatively constant during December–February when the upstream freshwater runoff was minimal, and decreased slightly in March, possibly signaling the onset of the spring freshet. More pronounced, however, is the difference between the two consecutive winters: OCCC water was 0.2 fresher in January–March 2005 than during the same

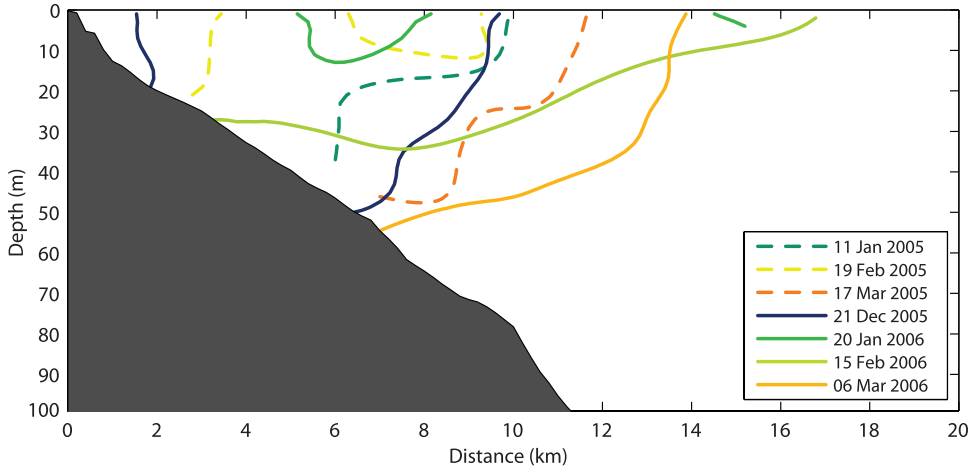

Figure 6. Evolution of the frontal position in the winters of 2005 and 2006. Isopycnals corresponding to maximum surface density gradient are shown. Properties of the front are given in Table 2.

period the following year. This difference is the opposite of what could be expected from the river discharge data (see section 2.4) that showed much greater freshwater runoff during the second season of observations. Such a discrepancy suggests that the observed change in salinity may be related to variability in the Scotian shelf freshwater input.

[41] Salinity offshore of the OCCC exhibited even stronger variations during the two winters of observations. For the purpose of this study we define the ambient salinity S_0 as the salinity averaged over the rectangle 13 to 15 km offshore and 40–60 m below the surface. As can be seen from Figure 6, this region was outside of the OCCC wedge at all times. At the same time it is shallow enough to be within the relatively homogeneous seasonal mixed layer.

[42] The difference between the OCCC and the ambient salinity increased in February–March during both years (Figure 7). In 2006, offshore salinity actually increased as the coastal current salinity dropped, while in 2005 both decreased, but at different rates. As a result, the salinity contrast across the OCCC front increased by a factor of 3 from January to March 2006, and by a factor of 1.4 during the same period of 2005. Thus the density contrast is driven by both the evolution of the OCCC water mass adjacent to the coast as well as the larger-scale shifts in water masses in the interior basins of the Gulf of Maine.

3.3. Density Stratification

[43] Density stratification of the midshelf in winter was primarily governed by salinity: $|(\partial\rho/\partial S)\Delta S|$ was approximately four times greater than $|(\partial\rho/\partial T)\Delta T|$, where ΔS and ΔT are typical salinity and temperature differences. In early winter (December–January) the density anomaly of the coastal current was at its seasonal low, $\Delta\rho$ = 0.1–0.15 kg m^{-3} (Figure 8). It is interesting, that even though the OCCC water salinity was about 0.2 higher during the 2006 season (Figure 7), the density difference between the OCCC and ambient waters was the same during the early parts of both field seasons. Following the freshening of the coastal current and increasing ambient salinity (see section 3.2), the density anomaly of the OCCC increased each year, reaching 0.2 kg m^{-3} by 15 March 2005, and 0.4 kg m^{-3} by 6 March 2006.

[44] Vertical stratification changed with the changing slope of the coastal current front. During upwelling-favorable winds, when the wedge of the OCCC water was stretched over a large distance (e.g., on 15 February 2006, see Figure 6), the buoyancy frequency below the plume reached 0.02 s^{-1}. Upon upwelling relaxation, the maximum buoyancy frequency decreased to 0.007–0.014 s^{-1}. Outside the coastal current, the ambient buoyancy frequency in the top 60 m was typically less than 0.003 s^{-1}.

3.4. Velocity Structure

[45] Dynamics of the Gulf of Maine shelves are controlled by buoyancy, wind and tides in roughly equal proportion [*Brown and Irish*, 1992].

[46] The density difference across the coastal current front creates a baroclinic pressure gradient that supports

Table 2. Coastal Current Front Properties[a]

Date	x_f (km)	σ_f (kg m^{-3})	α ($\times10^{-3}$)	$\Delta\sigma$ (kg m^{-3})	τ_y ($\times10^{-2}$ Pa)
11 Jan 2005	10.0	25.3	−4.9	0.12	−7.7
19 Feb 2005	3.4	25.5	−38.8	0.07	−1.9
17 Mar 2005	11.7	25.4	−9.8	0.21	−1.6
21 Dec 2005	9.7	25.3	−14.4	0.15	−5.5
20 Jan 2006	8.2	25.3	−0.6	0.14	9.5
15 Feb 2006	16.8	25.6	−2.3	0.33	5.3
6 Mar 2006	13.9	25.8	−6.4	0.43	−5.9

[a]Location of maximum cross-shore surface density gradient (x_f), frontal isopycnal (σ_f), mean slope of the frontal isopycnal (α), change of potential density across the front ($\Delta\sigma$), and along-shore wind stress averaged over the previous 6 h (τ_y). Positive τ_y corresponds to northward (upwelling favorable) wind.

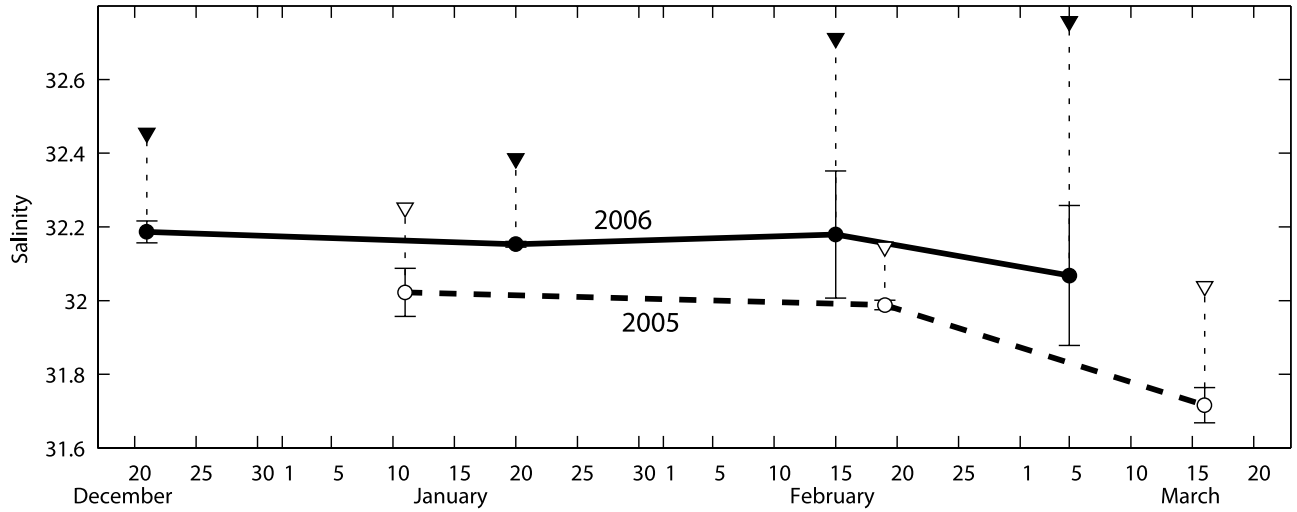

Figure 7. Wintertime evolution of the salinity on the Outer Cape Cod shelf. Section averages of the OCCC water salinity (circles and thick lines) are shown for 2 years of observations: 2005 (open symbols) and 2006 (filled symbols). Triangles indicate contemporaneous observed ambient offshore salinity values. Coastal current is defined (hydrographically) as the volume enclosed within the frontal isohalines shown in Figure 6. Error bars represent standard deviation of the OCCC water salinity values, observed during each survey.

geostrophically balanced along-shore flow. This is the only forcing factor intrinsic to the coastal current itself. Evidence of the buoyancy-driven baroclinic flow can be seen in the AUV velocity observations as a southward flowing surface-intensified jet in the vicinity of the OCCC front (Figure 4d). The strongest flow, reaching 0.3 m s^{-1}, was observed in association with a steeply sloping frontal configuration (e.g., 21 December 2005). Vertical shear of the buoyancy-driven flow can be generally captured by geostrophic calculations based on the observed horizontal density gradient (see comparison to both moored and REMUS ADCP profiles of along-shelf velocity in Figure 9).

[47] Wind-driven response of the midshelf circulation can be conceptually split into two parts: frictional Ekman layer dynamics, and the interior geostrophic flow. The latter is supported by the barotropic cross-shore pressure gradient arising from the nearshore divergence of the Ekman transport, and the large-scale wind stress curl. Redistribution of the density field by the cross-shore advection may also alter the baroclinic geostrophic flow.

[48] The interior wind-driven barotropic flow was clearly visible in the bottom-mounted ADCP record. Subtidal along-shore velocities observed in February–March 2006 were strongly correlated with the along-shore winds, reported by the offshore buoy (Figure 10). Maximum

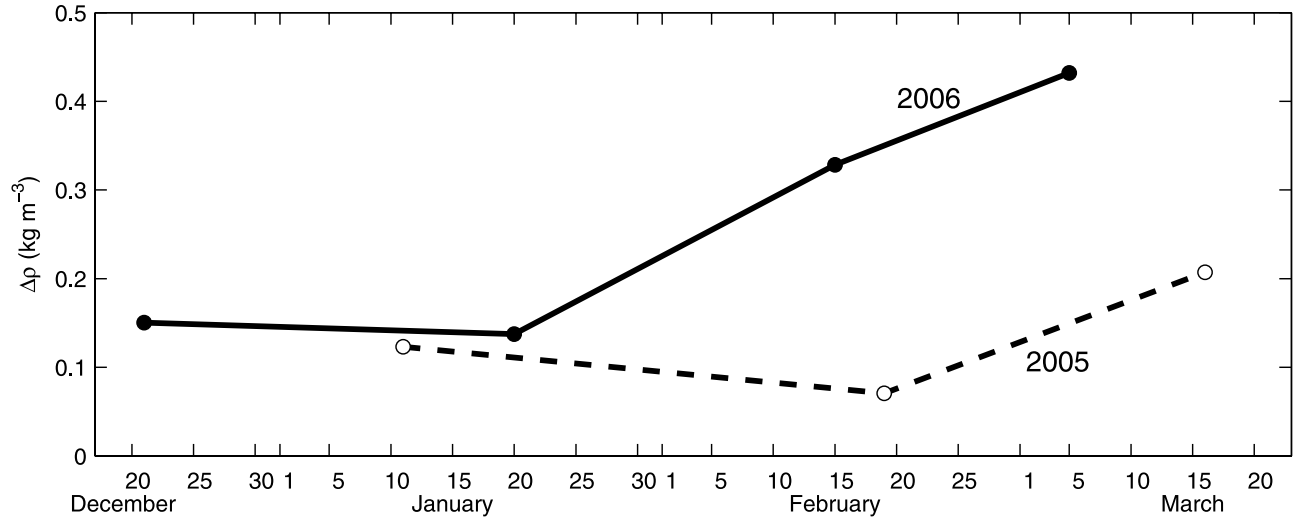

Figure 8. Density anomaly of the coastal current, defined as the difference between the section-averaged densities of the ambient and OCCC waters. Two years of observations are shown: 2005 (open symbols) and 2006 (filled symbols).

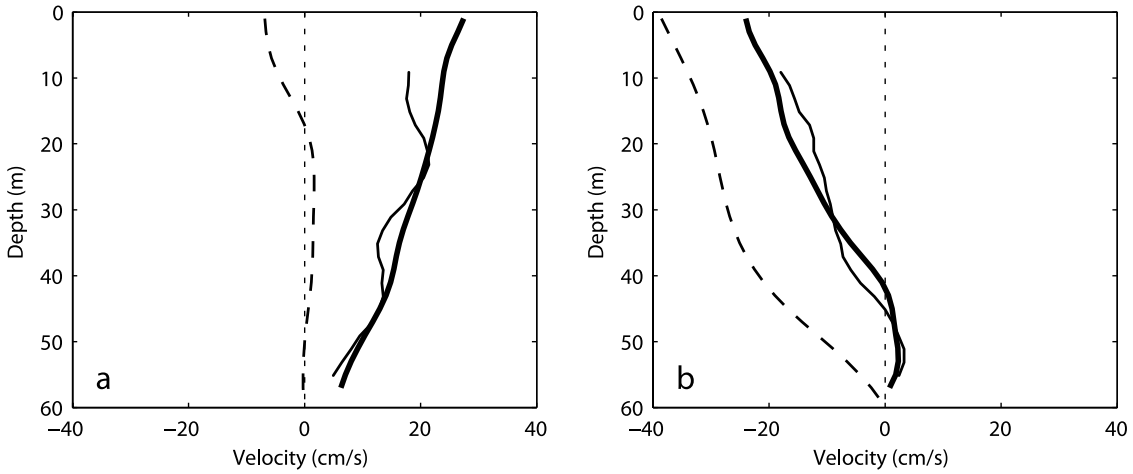

Figure 9. Examples of vertical profiles of along-shore velocity at the 60-m isobaths mooring site during the AUV "fly-bys" on (a) 15 February and (b) 6 March 2006. AUV (thick solid line) and bottom-mounted ADCP (thin solid line) observations are shown, together with the bottom-referenced geostrophic velocity profile (dashed line). Tidal signal has been removed from the observations.

correlation was achieved at a lag of about 1/2 of the inertial period (9 h) and was uniformly high (>0.6, significant at over 99%) throughout the water column. The remainder of the barotropic flow, not correlated with the local wind could be attributed to the large-scale factors driving the Gulf of Maine gyre circulation, including remote wind patterns and tidal rectification [*Brown and Irish*, 1992].

[49] Ekman layer transport could not be observed directly with the bottom-mounted ADCP owing to the near-surface interference. The flow in the top bins was strongly correlated with the along-shore wind at near-zero lag (Figure 10b), which would be consistent with the frictional flow. The absence of such correlation in the cross-shore flow, however, suggests that the ADCP signal in the near-surface bins was affected by the surface wave scattering of the ADCP signal rather than the Ekman flow. Vertically integrated along-shore Ekman layer transport could be estimated indirectly from the wind observations as

$$V_{Ek} = -\tau_x(\rho_0 f)^{-1}, \quad (1)$$

where τ_x is the cross-shore wind stress, $\rho_0 = 1025$ kg m^{-3} is the nominal density, and $f = 9.8 \times 10^{-5}$ s^{-1} is the Coriolis parameter. During the winter storms, southward Ekman layer transport routinely exceeded 5 m^2 s^{-1}.

[50] The Outer Cape Cod region is characterized by moderately strong tides. On the basis of the harmonic analysis of the limited moored velocity observations, we found semidiurnal M2 component to be dominant (major axis of the tidal ellipse 0.23 m s^{-1}). The next-largest constituents were N2 and S2 (with the major axes of 0.06 and 0.04 m s^{-1}, respectively). Combined tidal flow amplitude exceeded 0.3 m s^{-1} during spring tides.

[51] The following section focuses on subtidal variability of along-shore freshwater transport. A local tidal prediction based on the high-resolution Finite Volume Coastal Ocean Model (FVCOM) run for the Gulf of Maine region (C. Chen, personal communication, 2006) was subtracted from the AUV and moored velocity observations. The model prediction of the local tidal flow compared favorably with the moored ADCP velocity observations: root-mean square

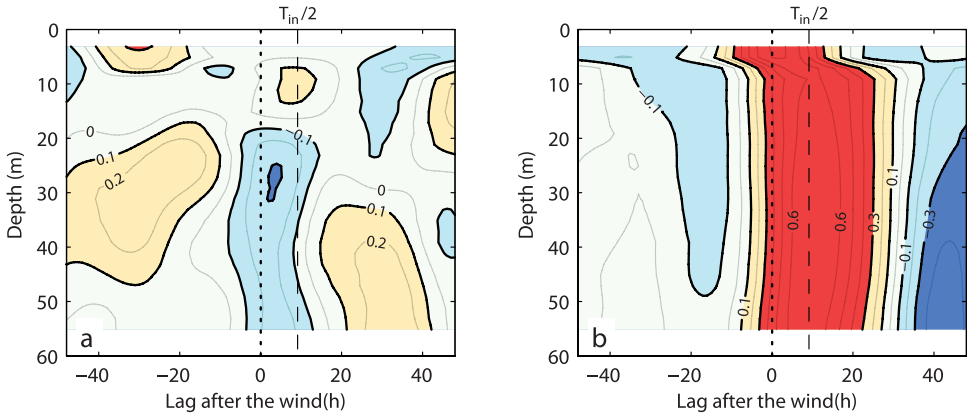

Figure 10. Lagged correlations of the along-shore wind with (a) cross-shore and (b) along-shore velocity measured by the bottom-mounted ADCP. Vertical dashed lines mark one half of the inertial period (18/2 = 9 h). All time series were band-passed with the half-power limits of 24 and 240 h.

(RMS) errors of the model prediction of the along- and cross-shore components of the barotropic tide were 0.05 m s^{-1} and 0.03 m s^{-1}, respectively. The tidal model overestimated the variance in the along-shore tide component by 18%, which is equivalent to a 7% amplitude overestimation.

4. Freshwater Transports

[52] Given the information of the cross-shelf distribution of along-shore velocity v and salinity S, the freshwater transport of the coastal current can be estimated as an integral of the product of salinity anomaly and cross-section velocity over the area of the section A [*Brown and Irish*, 1993; *Geyer et al.*, 2004],

$$Q = \int\int_A v\frac{S_0 - S}{S_0}dxdz, \tag{2}$$

where S_0 is the ambient salinity outside the coastal current (see section 3.2). For each hydrographic survey, (2) can be integrated directly. The resulting value, however, may not be synoptically representative since the forcing situation itself may not be typical. In order to estimate freshwater transport evolution between the surveys, contributions due to baroclinic geostrophic flow (Q_{bc}), barotropic wind-driven flow (Q_{bt}), and frictional Ekman layer flow (Q_{Ek}) were treated separately.

[53] Thermohaline structure of shelf waters as well as the associated baroclinic circulation varies slowly (characteristic timescale greater than 20 days [*Brown and Irish*, 1993]). Consequently, evolution of baroclinic freshwater transport can be adequately represented by temporal interpolation between the values of Q_{bc}, calculated for each AUV survey as

$$Q_{bc} = \int\int_A v_{bc}\frac{S_0 - S}{S_0}dxdz, \tag{3}$$

where v_{bc} is the baroclinic geostrophic velocity field. Reference velocity in geostrophic calculations was chosen such that the vertical average of v_{bc} vanished. Baroclinic transport Q_{bc} includes both the buoyancy-driven flow and the secondary wind-driven flow that results from the distortion of the density field by cross-shore circulation.

[54] Barotropic wind-driven shelf response is highly variable (typical timescales of 2 to 20 days [*Brown and Irish*, 1993]), but relatively uniform over the coastal current region. We derived the time record of barotropic flow evolution v_{bt} from the depth average of the bottom-mounted ADCP record (corrected for tidal effects). Note that v_{bt} also included the large-scale barotropic pressure gradient contribution which is expected to vary slowly both in space and in time. Since v_{bt} is assumed to be spatially uniform, barotropic freshwater transport contribution is given by

$$Q_{bt} = v_{bt}\int\int_A \frac{S_0 - S}{S_0}dxdz. \tag{4}$$

[55] Section integral of the normalized salinity anomaly can be seen as an equivalent freshwater cross section $A_{FW} = \int\int_A (S_0 - S)S_0^{-1}dxdz$. This parameter varies slowly with the changing salinity anomaly of the coastal current (note that it is not affected by the change of the shape of the CC "wedge"), and could also be approximated by temporal interpolation between the hydrographic surveys. Barotropic freshwater transport estimates were only available for the second half of the deployment when the bottom-mounted ADCP was operational.

[56] Direct Ekman transport associated with the cross-shore wind can also contribute to the along-shore flow in the upper few meters of the water column. Since the freshwater anomaly associated with the coastal current reaches its maximum near the surface, the resulting freshwater transport can be of the same order as that due to the other forcing terms [*Geyer et al.*, 2004]. If the salinity is constant across Ekman layer and the wind stress is spatially uniform, then the along-shore Ekman freshwater transport can be found by integration over the section length L,

$$Q_{Ek} = V_{Ek}\int_L \frac{S_0 - S_s}{S_0}dx = V_{Ek}L_{FW}, \tag{5}$$

where S_s is the surface salinity, and L_{FW} is the "effective freshwater length," defined as the section integral of normalized surface salinity anomaly,

$$L_{FW} = \int_L \frac{S_0 - S_s}{S_0}dx. \tag{6}$$

[57] Unlike A_{FW} introduced above, L_{FW} can be expected to be partially correlated with the along-shore wind (or, more precisely, with the along-shore wind stress time integral): as was shown in section 3.2, northward (upwelling favorable) wind stretches the coastal current plume thus increasing L_{FW}, and vice versa. In present study, however, we can do no better than interpolating between the values of L_{FW}, observed during the AUV surveys, effectively disregarding the possibility of its high-frequency variation. It should be noted that Q_{ek} is not entirely independent of the barotropic transport Q_{bt} defined above, since the Ekman layer flow may be partially registered by the bottom-mounted ADCP. No characteristic flow veering associated with the Ekman spiral was observed in the top valid bins of the ADCP record, so the contribution of Q_{ek} to Q_{bt} is expected to be weak.

[58] Assessment of freshwater transport for the 2006 season are summarized in Figure 11, showing both the direct estimates based on hydrographic surveying and the projected contributions of baroclinic, barotropic, and Ekman transports, calculated according to (3)–(5). A similar comparison for the 2005 season could not be made owing to the lack of long-term velocity measurements. The direct transport measurements based on 2005 AUV surveys were within the estimation error and thus inconclusive.

[59] Freshwater transport on the Outer Cape Cod shelf in February and March 2006 was dominated by barotropic flow. Mean southward transport based on (3)–(5) was $1.1 \pm 0.3 \times 10^3$ m^3 s^{-1} in February and $1.8 \pm 0.4 \times 10^3$ m^3 s^{-1} in the first half of March (see Appendix A for the details of uncertainty estimation). These values are consistent with the estimates of *Geyer et al.* [2004] and *Chen et al.* [1995b]. Oscillations of the flow, largely attributable to the barotropic

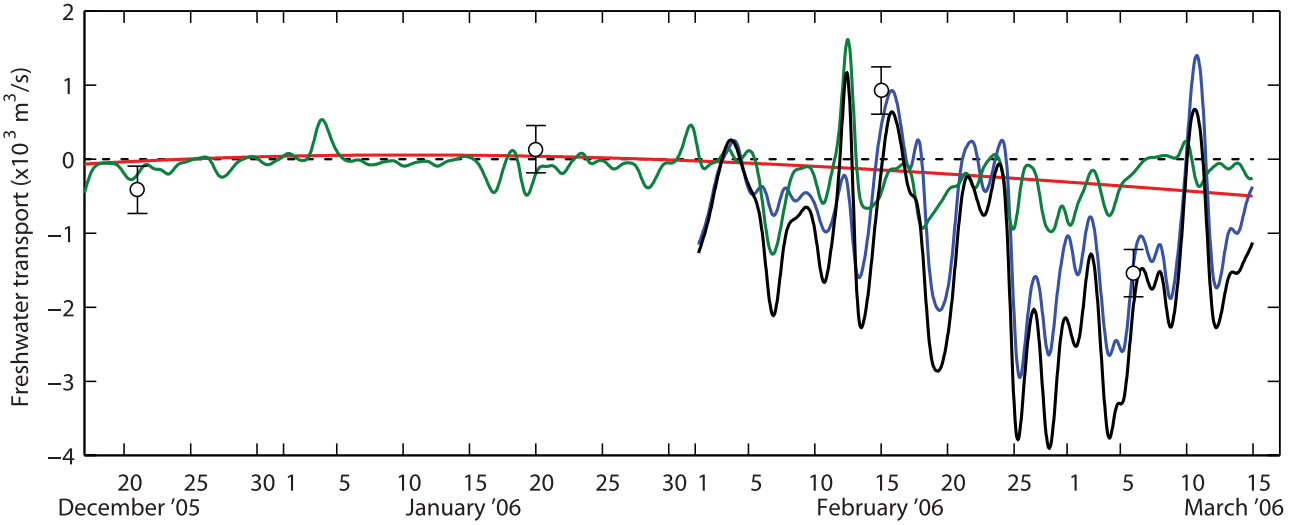

Figure 11. Alongshore OCCC freshwater transport during the 2006 season. Direct estimates based on AUV observations are shown by circles, with the error bars representing the uncertainty of the estimates (see Appendix A). The thick black line shows estimated freshwater transport evolution (low-passed with 2-day Blackman filter). Thin lines show respective contributions of baroclinic (Q_{bc}, red), barotropic (Q_{bt}, blue), and Ekman (Q_{Ek}, green) transports.

component variability, occasionally reversed the alongshore freshwater transport direction. One of such reversals during the upwelling event on 15–17 February 2006 was also confirmed by the AUV survey.

[60] Baroclinic freshwater transport was generally weak, despite relatively high velocities associated with it (see section 3.4). In the first half of March 2006 it strengthened to -0.5×10^3 m^3 s^{-1}, which was still less than 30% of the mean freshwater transport during that period. Buoyancy-driven contribution to OCCC freshwater transport is expected to increase further by late spring, as the OCCC water becomes fresher and the southward winds weaken. *Geyer et al.* [2004] concluded that even in spring the baroclinic contribution to the freshwater transport in WMCC is smaller than the barotropic flow. Further study of this transition in OCCC is consequently desirable.

[61] The Ekman component of the freshwater transport was comparable with buoyancy-driven contribution (-0.3×10^3 m^3 s^{-1} on average in February–March 2006). During certain storms (notably 7 and 12 February 2006), Ekman freshwater transport increased sharply to $\pm 1 \times 10^3$ m^3 s^{-1} and dominated over the buoyancy-driven and even barotropic components.

[62] *Whitney and Garvine* [2005] parameterized the importance of the local wind influence on the coastal current using the wind strength index

$$W_S = v_{wind}/v_{dis},$$

where v_{wind} and v_{dis} are the wind- and buoyancy-driven along-shelf flow velocities. This parameter, however, does not adequately represent contribution of the two forcing mechanisms to the along-shore transport. Since the buoyancy-driven flow is concentrated near the density front, it transports substantially less volume than the wind-driven flow of the same velocity advecting the coastal current plume as a whole. The difference is even more pronounced if we consider freshwater transport, since the maximum salinity anomaly is typically observed close to the shore in the region of weak buoyancy-driven flow. To reflect this difference, a slightly modified wind strength index can be defined for the purpose of this study as

$$W_Q = (Q_{bt} + Q_{Ek})/Q_{bc}.$$

(Here we assume that the barotropic freshwater transport Q_{bt} is entirely wind-driven, which is reasonable, given its high correlation with the local wind, demonstrated in section 3.4. It should be noted, however, that large-scale wind patterns, tidal rectification, and inflow imbalance also contribute to Q_{bt}.) In our observations W_Q varied from 1 to 30, with the average value of 7.2, suggesting general predominance of the wind-driven freshwater transport over the buoyancy-driven one. It is interesting that the OCCC maintained its integrity despite almost negligible baroclinic transport. In fact, the weakness of baroclinicity of the OCCC in winter may have contributed to its unexpected stability, discussed in section 5.

5. Discussion

[63] A plume of buoyant coastal current water has a range of potential impacts on wintertime water mass modification on the shelf. We will now discuss two factors that may have made the persistence of OCCC and other Gulf of Maine coastal currents relevant to the problem of MIW formation: reduction of maximum attainable density and inhibition of cross-shore eddy fluxes. Another factor, alteration of vertical buoyancy- and wind-driven overturning, is addressed in the accompanying paper (Shcherbina and Gawarkiewicz, submitted manuscript, 2008).

[64] Continual presence of the freshwater anomaly near the shore limited the maximum density attainable by wintertime cooling. Even if cooled to the freezing point, the

OCCC water, observed during the 2005 and 2006 winters, would only reach density of 25.7–25.9 kg m^{-3}. This is substantially lower than the density of the deep MIW (26.2 kg m^{-3}). Consequently, the inner shelf water could not ventilate the deep MIW in the process suggested by *Mupparapu and Brown* [2002]. Our observations, however, do not exclude the possibility of such ventilation during some anomalous winters. In the absence of OCCC, the maximum attainable density (at the ambient mixed layer salinity and freezing temperature) would have reached 26.4 by March 2006, well beyond the MIW density range. The presence of the coastal current, however, pushed the saltier water away from the coast where it did not undergo sufficient cooling owing to the greater water depth. It is unclear what winter nearshore salinities have been in the past when runoff from rivers in the western Gulf of Maine may not have contributed fresh water to the system through the winter. Our observations do not preclude the nearshore formation of dense waters in previous years or decades.

[65] Presence of the coastal current front also reduced cross-shelf exchange. Numerical models and direct observations have identified eddy fluxes as a key mechanism to transport the newly formed intermediate water offshore [*Gawarkiewicz and Chapman*, 1995; *Pringle*, 2001; *Shcherbina et al.*, 2004]. A combination of sloping bottom with the positive cross-shore density gradient associated with the buoyant plume changes the stability characteristics of the coastal zone. As a result of this stabilization, the eddy transport may be reduced.

[66] A simple estimate of the impact of the sloping bottom on the stability of the coastal current can be made by applying quasi-geostrophic linear stability theory [*Blumsack and Gierasch*, 1972; T. Stipa, On the sensitivity of coastal quasigeostrophic edge wave interaction to bottom boundary characteristics: Possible implications for eddy parameterizations, arXiv:physics/0401119, 2004]. The analysis implies a basic state with uniformly sloping isopycnals over a sloping bottom and allows for a simple parameterization of the instability timescales for gently sloping topography and small Rossby numbers. Many assumptions of the theory are violated in the coastal current setting (e.g., variation of topography is the same order as the water depth, Rossby number is of the order of 1, density and velocity gradients are not linear, bottom stress is not negligible). Nonetheless, it is useful for gaining insight into the relative stability of the various density structures.

[67] A key parameter determining stability of the system is the ratio δ between the bottom and isopycnal slopes. A flat bottom case (the so-called Eady problem) corresponds to $\delta = 0$; it is baroclinically unstable for the widest range of nondimensional wave numbers. Dense plumes tend to have $\delta \geq 0$ owing to the intense vertical mixing which results in nearly vertical isopycnals. In this case, the longest waves are stabilized, but the rate of growth of the disturbances with intermediate wavelength increases. This explains the rapid dispersal of dense plumes by the baroclinic eddy field [*Gawarkiewicz and Chapman*, 1995; *Pringle*, 2001; *Shcherbina et al.*, 2004]. On the other hand, for the case of a buoyant plume, the isopycnals and the bottom are inclined in the opposite directions, so that $\delta < 0$. Such slope also stabilizes long waves, but also increases the wavelength of the dominant instability, and reduces the instability growth rate [*Blumsack and Gierasch*, 1972]. Overall, $\delta < 0$ results in the most stable configuration.

[68] Typical density field in the OCCC region (Figure 4c) corresponds to $\delta \approx -1$. The maximum instability growth rate for this configuration is about 50% of that for the flat-bottom or dense-plume cases. To estimate the dimensional timescale of the instability for the OCCC case, we assume the reduced gravity of $g' = 4.8 \times 10^{-3}$ m s^{-2}, corresponding to a cross-front density difference of 0.5 kg m^{-3}, typical cross-shelf scale of $L = 7$ km, the mean water depth of $H = 60$ m, and the Coriolis parameter of $f = 9.8 \times 10^{-5}$ s^{-1}. These parameters give the nondimensional Burger number

$$B = g'H(fL)^{-2} = 0.59,$$

and the e-folding timescale for the instability growth of 27 h, compared to 12 h for the flat bottom case. The most unstable wavelength is reduced to 11 km for $\delta = -1$, compared to 21 km for the case of flat bottom.

[69] Even though the quasi-geostrophic theory explains the improved stability of the OCCC over the flat-bottom and the dense-plume configurations, it still predicts a relatively short instability growth timescale. As the advection time from the closest substantial source of fresh water (Merrimack river) is about 200 h and the path along the western shore of Cape Cod takes 60 h (assuming steady 0.2 m s^{-1} current speed), one would expect to see a well-developed eddy field in the OCCC. In reality, virtually no hydrographic surveying or examination of satellite sea surface temperature imagery revealed any instances of obvious eddy formation or detachment (a notable exception is the REMUS survey of 6–7 March 2006, showing a sign of eddy activity). It is possible that the fairly constant wind-forcing imposes different length scales on the coastal current that prevent instabilities growing, or that bottom friction prevents growth of any instabilities. *Stipa* [2004] observed similarly anomalous persistence of a coastal current in the Gulf of Finland. He found no satisfactory explanation for why analytical stability theory fails to predict the emergence of such quasi-stable state, but speculated that the effects of nonlinearity or Ekman transport in the bottom boundary layer may play important role in stabilizing the current under some circumstances. Further research on the alternative stabilizing mechanisms that would allow a coastal current to preserve its integrity over a long path is certainly warranted.

[70] We also note that in our study, just like in many other cases [e.g., *Rudels et al.*, 2000; *Stipa*, 2004; *Whitney and Garvine*, 2005], a quasi-stable coastal current exhibits the ratio of the isopycnal slope to the bottom slope close to $\delta = -1$. It is interesting to speculate that there might be some form of dynamical control that leads to this relation as a preferred structure for coastal currents in general.

6. Conclusions

[71] Our observations in the Outer Cape Cod Coastal Current during the winters of 2005 and 2006 revealed complex and variable thermohaline structure. Despite strong cooling and mixing, both the vertical and horizontal density gradients associated with the buoyant plume persisted throughout the winters, even though the study region was

considerably removed from both terrestrial and oceanic freshwater sources.

[72] Density anomaly of the plume varied from 0.1 kg m^{-3} in 2005 to 0.4 kg m^{-3} in spring of 2006, responding to the changing freshwater runoff in the Gulf of Maine. Offshore extent of the OCCC water was marked by a weak front, typically intersecting the bottom between the 40- and 60-m isobaths (6–8 km offshore). The front sloped upward as it extended offshore and outcropped at the surface 10–14 km from the coast. During the periods of strong northward (upwelling favorable) winds the freshwater plume moved seaward and extended more than 16 km offshore. The front was associated with a narrow surface-intensified southward current, with maximum velocities reaching 30 cm s^{-1}in a surface-trapped frontal jet.

[73] Wintertime along-shore freshwater transport was controlled by highly variable barotropic flow driven by local winds and large-scale pressure gradient. Mean southward freshwater transport was $1.1 \pm 0.3 \times 10^3$ m^3 s^{-1} in February and $1.8 \pm 0.4 \times 10^3$ m^3 s^{-1} in the first half of March 2006. Despite the intensity of baroclinic buoyancy-driven flow, its contribution to the freshwater transport was typically an order of magnitude smaller.

[74] The observations described here suggest that the persistence of a coastal current throughout the winter has a major impact on water mass formation processes in shallow water. Freshwater anomaly retained near the coast reduces the maximum density of the shelf water attainable by winter cooling. Additionally, the coastal current front may inhibit cross-shelf export of cold water from the inner shelf zone to the stratified interior of adjacent basins.

[75] We also note that this coastal current is an important choke point for flow exiting the Gulf of Maine to both the northern flank of Georges Bank and Nantucket Shoals to the Middle Atlantic Bight. The maximum buoyancy-driven transport in the spring was 0.09 Sv, which is nearly one quarter of the annual mean transport across the shelf south of Nantucket Shoals [*Beardsley et al.*, 1985]. We thus encourage future consideration of this region as a site for a sustained ocean observing system that would efficiently monitor water mass variability and along-shelf fluxes of fresh water and nutrients into both the Georges Bank region and Middle Atlantic Bight.

Appendix A: Uncertainty of the Transport Estimate

[76] The uncertainty ΔQ of direct freshwater transport estimation based on AUV data can be roughly estimated by propagating the intrinsic error of the REMUS ADCP velocity measurements Δv_A and the error contribution of the tidal model Δv_T through the equation (2):

$$\Delta Q \approx \overline{A_{FW}} \left[(\Delta v_A)^2 + (\Delta v_T)^2 \right]^{1/2},$$

where $\overline{A_{FW}} = 4.6 \times 10^3$ m^2 is the average value of integrated relative salinity anomaly $A_{FW} = \int \int_A (S_0 - S) S_0^{-1} \, dxdz$. The base error of REMUS velocity measurement Δv_A is difficult to quantify. In shallow water, where the bulk of the freshwater transport occurs, we expect the error to be minimal, since the ADCP bottom tracking information is readily available there. In deeper water, the relative contribution of dead reckoning errors increases. Overall, the value of $\Delta v_A = 0.05$ m s^{-1} can be used as a conservative estimate of the RMS error of the REMUS velocity data. The tidal model also showed a RMS error of $\Delta v_T = 0.05$ m s^{-1} when compared with the bottom-mounted ADCP observations. Even though the errors can potentially be different at other locations along the section, the above value can still be used as a rough estimate. This gives the error of the freshwater transport estimate $\Delta Q = 0.3 \times 10^3$ m^3 s^{-1}.

[77] Uncertainty in the estimates of monthly mean values of freshwater transport $\overline{Q}$ arises chiefly from the variability of the signal itself. Standard deviation of the estimate of the mean is given by

$$\sigma_{\bar{Q}} = N_{DOF}^{-1/2} \sigma_Q,$$

where $\sigma_Q = 1.3 \times 10^3$ m^3 s^{-1} is the standard deviation of the transport time series, and N_{DOF} is the number of degrees of freedom of the estimate (i.e., the number of statistically independent realizations of Q that participate in the average). Averaging over a time window of length T contributes $N_{DOF} = T/T_0$ degrees of freedom toward the estimate of the mean transport value, where $T_0 = 32$ h is the decorrelation timescale of alongshore barotropic flow that controls variability of the transport. Thus, a 15-day average corresponds to $N_{DOF} \approx 11$, and its expected standard deviation is $\sigma_{\bar{Q}_{15}} \approx 0.4 \times 10^3$ m^3 s^{-1}. Correspondingly, the standard deviation of a monthly average is $\sigma_{\bar{Q}_{30}} \approx 0.3 \times 10^3$ m^3 s^{-1}.

[78] **Acknowledgments.** This work was supported by the Coastal Ocean Institute of the Woods Hole Oceanographic Institution and the WHOI SeaGrant Office under grant NA06OAR4170021. G.G. was supported by the Office of Naval Research as part of the AWACS program under grant N00014-05-1-0410. A.S. was supported, in part, by WHOI Post-Doctoral Scholarship. We thank Captain Ken Houtler and Chief Mate Ian Hanley for getting *Tioga*, REMUS, and ourselves through some rough seas; Craig Marquette is thanked for designing and deploying the moorings. Chris Linder and Al Plueddemann also went along on several of the cruises and assisted in the interpretations of the results. Thanks go to both the Oceanographic Systems Laboratory at WHOI and Hydroid Inc. who have helped us enormously in learning how to use our REMUS vehicle in challenging environments. The FVCOM tidal model was provided by Changsheng Chen and coworkers at the University of Massachusetts-Dartmouth. Satellite thermal imagery was provided by the Coastal Ocean Observing Laboratory and Marine Remote Sensing Lab at Rutgers University.

References

Beardsley, R. C., D. C. Chapman, K. H. Brink, S. R. Ramp, and R. Schlitz (1985), The Nantucket Shoals Flux Experiment (NSFE79). Part I: A basic description of the current and temperature variability, *J. Phys. Oceanogr.*, *15*, 713–748, doi:10.1175/1520-0485(1985)015<0713:TNSFEP>2.0.CO;2.

Blanton, J. O., L. Y. Oey, J. Amft, and T. N. Lee (1989), Advection of momentum and buoyancy in a coastal frontal zone, *J. Phys. Oceanogr.*, *19*, 98–115, doi:10.1175/1520-0485(1989)019<0098:AOMABI>2.0.CO;2.

Blumsack, S. L., and P. J. Gierasch (1972), Mars: The effects of topography on baroclinic instability, *J. Atmos. Sci.*, *29*, 1081–1089, doi:10.1175/1520-0469(1972)029<1081:MTEOTO>2.0.CO;2.

Brown, W. S., and R. C. Beardsley (1978), Winter circulation in the western Gulf of Maine: Part 1. Cooling and water mass formation, *J. Phys. Oceanogr.*, *8*, 265–277, doi:10.1175/1520-0485(1978)008<0265:WCITWG>2.0.CO;2.

Brown, W. S., and J. D. Irish (1992), The annual evolution of geostrophic flow in the Gulf of Maine: 1986–1987, *J. Phys. Oceanogr.*, *22*, 445–473, doi:10.1175/1520-0485(1992)022<0445:TAEOGF>2.0.CO;2.

Brown, W. S., and J. D. Irish (1993), The annual variation of water mass structure in the Gulf of Maine: 1986–1987, *J. Mar. Res.*, *51*(1), 53–107, doi:10.1357/0022240933223828.

Brown, W. S., J. Vermersch, and R. C. Beardsley (1977), Wintertime 1974–75 Western Gulf of Maine Experiment data, *Tech. Rep. WHOI-77–22*, 95 pp., Woods Hole Oceanogr. Inst., Woods Hole, Mass.

Chapman, D. C., and S. J. Lentz (1994), Trapping of a coastal density front by the bottom boundary layer, *J. Phys. Oceanogr.*, *24*, 1464–1479, doi:10.1175/1520-0485(1994)024<1464:TOACDF>2.0.CO;2.

Chen, C., R. C. Beardsley, and R. Limeburner (1995a), Variability of water properties in late spring in the northern Great South Channel, *Cont. Shelf Res.*, *15*(4–5), 415–431, doi:10.1016/0278-4343(94)00054-Q.

Chen, C., R. C. Beardsley, and R. Limeburner (1995b), Variability of currents in late spring in the northern Great South Channel, *Cont. Shelf Res.*, *15*(4–5), 451–473, doi:10.1016/0278-4343(94)00056-S.

Csanady, G. T. (1978), Wind effects on surface to bottom fronts, *J. Geophys. Res.*, *83*, 4633–4640, doi:10.1029/JC083iC09p04633.

Fairall, C. W., E. F. Bradley, J. E. Hare, A. A. Grachev, and J. B. Edson (2003), Bulk parameterization of air-sea fluxes: Updates and verification for the COARE algorithm, *J. Clim.*, *16*(4), 571–591, doi:10.1175/1520-0442(2003)016<0571:BPOASF>2.0.CO;2.

Fong, D. A., W. R. Geyer, and R. P. Signell (1997), The wind-forced response on a buoyant coastal current: Observations of the western Gulf of Maine plume, *J. Mar. Syst.*, *12*(1–4), 69–81, doi:10.1016/S0924-7963(96)00089-9.

Franks, P., and D. Anderson (1992), Alongshore transport of a toxic phytoplankton bloom in a buoyancy current: Alexandrium tamarense in the Gulf of Maine, *Mar. Biol. Berlin*, *112*, 165–174, doi:10.1007/BF00349740.

Garvine, R. W. (2004), The vertical structure and subtidal dynamics of the inner shelf off New Jersey, *J. Mar. Res.*, *62*(3), 337–371, doi:10.1357/0022240041446182.

Gawarkiewicz, G., and D. Chapman (1995), A numerical study of dense water formation and transport on a shallow, sloping continental shelf, *J. Geophys. Res.*, *100*, 4489–4507, doi:10.1029/94JC01742.

Geyer, W. R., R. P. Signell, D. A. Fong, J. Wang, D. M. Anderson, and B. A. Keafer (2004), The freshwater transport and dynamics of the western Maine coastal current, *Cont. Shelf Res.*, *24*(12), 1339–1357, doi:10.1016/j.csr.2004.04.001.

Hopkins, T. S., and N. Garfield (1979), Gulf of Maine Intermediate Water, *J. Mar. Res.*, *37*(1), 103–109.

Kirincich, A. R., J. A. Barth, B. A. Grantham, B. A. Menge, and J. Lubchenco (2005), Wind-driven inner-shelf circulation off central Oregon during summer, *J. Geophys. Res.*, *110*, C10S03, doi:10.1029/2004JC002611.

Kundu, P. K., and J. S. Allen (1976), Some three-dimensional characteristics of low-frequency current fluctuations near the Oregon coast, *J. Phys. Oceanogr.*, *6*, 181–199, doi:10.1175/1520-0485(1976)006<0181:STDCOL>2.0.CO;2.

Lentz, S. J. (2001), The influence of stratification on the wind-driven cross-shelf circulation over the North Carolina shelf, *J. Phys. Oceanogr.*, *31*, 2749–2760, doi:10.1175/1520-0485(2001)031<2749:TIOSOT>2.0.CO;2.

Lentz, S., and K. Helfrich (2002), Buoyant gravity currents along a sloping bottom in a rotating fluid, *J. Fluid Mech.*, *464*, 251–278, doi:10.1017/S0022112002008868.

Lentz, S. J., and J. Largier (2006), The influence of wind forcing on the Chesapeake Bay buoyant coastal current, *J. Phys. Oceanogr.*, *36*, 1305–1316, doi:10.1175/JPO2909.1.

Lentz, S. J., and J. H. Trowbridge (1991), The bottom boundary layer over the northern California shelf, *J. Phys. Oceanogr.*, *21*, 1186–1201, doi:10.1175/1520-0485(1991)021<1186:TBBLOT>2.0.CO;2.

Lentz, S. J., and C. D. Winant (1986), Subinertial currents on the southern California shelf, *J. Phys. Oceanogr.*, *16*, 1737–1750, doi:10.1175/1520-0485(1986)016<1737:SCOTSC>2.0.CO;2.

Lynch, D. R., M. J. Holboke, and C. E. Naimie (1997), The Maine coastal current: Spring climatological circulation, *Cont. Shelf Res.*, *17*(6), 605–634, doi:10.1016/S0278-4343(96)00055-6.

Moline, M. A., S. M. Blackwell, C. von Alt, B. Allen, T. Austin, J. Case, N. Forrester, R. Goldsborough, M. Purcell, and R. Stokey (2005), Remote Environmental Monitoring Units: An autonomous vehicle for characterizing coastal environments, *J. Atmos. Oceanic Technol.*, *22*(11), 1797–1808, doi:10.1175/JTECH1809.1.

Mupparapu, P., and W. S. Brown (2002), Role of convection in winter mixed layer formation in the Gulf of Maine, February 1987, *J. Geophys. Res.*, *107*(C12), 3229, doi:10.1029/1999JC000116.

Pettigrew, N. R., D. W. Townsend, H. Xue, J. P. Wallinga, P. J. Brickley, and R. D. Hetland (1998), Observations of the Eastern Maine Coastal Current and its offshore extensions in 1994, *J. Geophys. Res.*, *103*, 30,623–30,639, doi:10.1029/98JC01625.

Pettigrew, N. R., J. H. Churchill, C. D. Janzen, L. J. Mangum, R. P. Signell, A. C. Thomas, D. W. Townsend, J. P. Wallinga, and H. Xue (2005), The kinematic and hydrographic structure of the Gulf of Maine Coastal Current, *Deep Sea Res., Part II*, *52*(19–21), 2369–2391, doi:10.1016/j.dsr2.2005.06.033.

Pringle, J. M. (2001), Cross-shelf eddy heat transport in a wind-free coastal ocean undergoing winter time cooling, *J. Geophys. Res.*, *106*, 2589–2604, doi:10.1029/2000JC900148.

Rennie, S. E., J. L. Largier, and S. J. Lentz (1999), Observations of a pulsed buoyancy current downstream of Chesapeake Bay, *J. Geophys. Res.*, *104*, 18,227–18,240.

Rudels, B., R. D. Muench, J. Gunn, U. Schauer, and H. J. Friedrich (2000), Evolution of the Arctic Ocean boundary current north of the Siberian shelves, *J. Mar. Syst.*, *25*(1), 77–99, doi:10.1016/S0924-7963(00)00009-9.

Shcherbina, A. Y., L. D. Talley, and D. L. Rudnick (2004), Dense water formation on the northwestern shelf of the Okhotsk Sea: 1. Direct observations of brine rejection, *J. Geophys. Res.*, *109*, C09S08, doi:10.1029/2003JC002196.

Signell, R. P., H. L. Jenter, and A. F. Blumberg (1996), Circulation and effluent dilution modeling in Massachusetts Bay: Model implementation, verification and results, *U. S. Geol. Surv. Open File Rep., 96–015*, 121 pp.

Smith, P. C. (1983), The mean and seasonal circulation off southwest Nova Scotia, *J. Phys. Oceanogr.*, *13*, 1034–1054, doi:10.1175/1520-0485(1983)013<1034:TMASCO>2.0.CO;2.

Stipa, T. (2004), Baroclinic adjustment in the Finnish coastal current, *Tellus, Ser. A*, *56*(1), 79–87.

Traykovski, P., A. E. Hay, J. D. Irish, and J. F. Lynch (1999), Geometry, migration, and evolution of wave orbital ripples at LEO-15, *J. Geophys. Res.*, *104*, 1505–1524, doi:10.1029/1998JC900026.

Whitney, M. M., and R. W. Garvine (2005), Wind influence on a coastal buoyant outflow, *J. Geophys. Res.*, *110*, C03014, doi:10.1029/2003JC002261.

Yankovsky, A., and D. Chapman (1997), A simple theory for the fate of buoyant coastal discharges, *J. Phys. Oceanogr.*, *27*, 1386–1401, doi:10.1175/1520-0485(1997)027<1386:ASTFTF>2.0.CO;2.

G. G. Gawarkiewicz, Woods Hole Oceanographic Institution, 266 Woods Hole Road, Woods Hole, MA 02543, USA.

A. Y. Shcherbina, Applied Physics Laboratory, University of Washington, 1013 NE 40th Street, Seattle, WA 98105, USA. (ashcherbina@apl.washington.edu)